

Detection of Dismounts using Synthetic Aperture Radar

J. Scott Goldstein¹, Michael L. Picciolo¹, Muralidhar Rangaswamy², Jacob D. Griesbach³

¹ManTech International Corp. Chantilly, VA, USA

²Air Force Research Laboratory, Sensors Directorate
Hanscom AFB, MA, USA

³Agilex, Colorado Springs, CO USA

Abstract— This paper presents an approach to detect people, or dismounts, using synthetic aperture radar (SAR). This approach is compared qualitatively with ground moving target indication (GMTI) radar and then quantitative results are presented using a P-band single phase center SAR. It is demonstrated that SAR provides an excellent methodology to detect dismounts.

I. INTRODUCTION

The detection of dismounts is paramount for many applications, including perimeter security, automobile safety systems, police surveillance, U.S. border patrol / Homeland Security and DoD purposes. The use of radar to detect dismounts is advantageous due to its all-weather, day-night operational capability. Radar dismount detection performance is often poor or even nonexistent when using single and multichannel ground moving target indication (GMTI) [1][2] radars. This poor performance is due to the signatures which humans exhibit being very different compared to the traditional targets that these radar systems were primarily designed to detect, such as vehicles and aircraft. In fact, dismount velocities are typically less than the minimum detectable velocity (MDV) of GMTI radars, exacerbating the problem of signal and clutter separation.

Traditionally, GMTI radar is designed to detect moving targets of appreciable radar cross section (RCS) by examining the target's reflected radar return, in either a monostatic or bistatic mode of operation. GMTI radar uses the Doppler frequency shift as a means for discriminating moving targets from stationary clutter. However, the detection of dismounts is very difficult for two fundamental reasons – the first is the relatively low RCS of the target, and the second is the small Doppler shift due to the low speed of dismounts. Of course, both of these properties compound the problem since this difficult target is only observed in the presence of ground clutter, whose radar return is often very strong.

A GMTI radar that attempts to detect a small RCS target with low Doppler will require exquisite hardware and complicated signal processing. The hardware will need to be very sensitive and a large number of antenna elements will be required to obtain both the accuracy and the resolution needed to detect dismounts. Space-time adaptive processing (STAP)

and other advanced algorithms (and associated processing power) will be necessary to mitigate clutter and detect the targets of interest [3][4][5].

Synthetic aperture radar (SAR) [6][7] is a mode of radar operation that achieves high resolution in the cross-range dimension by taking advantage of the motion of a moving platform carrying the radar to synthesize the effect of a large antenna aperture. In fact, the resolution of focused SAR is independent of range and depends on the dimension of the real antenna. SAR provides a radar map of the scene, i.e. the clutter, and the ground relief (due to hills or mountains) stands out because of the shadows they form. Thus there is context to a SAR image that naturally helps the interpretation of the scene, in contrast to GMTI synthetic detections (i.e., blips or dots) simply overlaid on a computer map display. In addition, SAR stereoscopic techniques can provide 3-D images of terrain, and SAR change detection processing can be applied to cancel clutter.

Since the SAR is designed to detect and focus stationary objects and clutter, moving objects will be extended in range and shifted and/or defocused (smeared) in the along-track dimension due to the motion of the target. However, these attributes also provide for a signature, since the physical mechanism that cause these effects are due to the target motion parameters themselves. In addition, a SAR image can be refocused based upon a different motion vector than the traditional zero velocity assumption for a fixed ground object.

SAR thus holds promise to be an advantageous and feasible way to detect dismounts instead of GMTI radar, especially if one is using an existing radar as opposed to designing a new and expensive one optimized for low RCS / low MDV targets. Other work in this area include [8][9]. This paper investigates the ability of SAR to detect dismounts by virtue of the unique dismount signatures present in SAR complex images, even for single phase center (i.e., single channel) SAR systems. Using advanced signal processing algorithms we present performance results for single channel SAR dismount detection using measured data from an operational UHF (P-band) SAR system.

This paper provides a brief review of GMTI and SAR systems to set context. The experimental setting for the SAR

This work was supported in part by the Electronic Systems Center through the Sensors Directorate of the Air Force Research Laboratory under contract number F33601-03-F-0203. Dr. Rangaswamy was supported by the Air Force Office of Scientific Research under project 2311HE.

Report Documentation Page

Form Approved
OMB No. 0704-0188

Public reporting burden for the collection of information is estimated to average 1 hour per response, including the time for reviewing instructions, searching existing data sources, gathering and maintaining the data needed, and completing and reviewing the collection of information. Send comments regarding this burden estimate or any other aspect of this collection of information, including suggestions for reducing this burden, to Washington Headquarters Services, Directorate for Information Operations and Reports, 1215 Jefferson Davis Highway, Suite 1204, Arlington VA 22202-4302. Respondents should be aware that notwithstanding any other provision of law, no person shall be subject to a penalty for failing to comply with a collection of information if it does not display a currently valid OMB control number.

1. REPORT DATE MAY 2010	2. REPORT TYPE	3. DATES COVERED 00-00-2010 to 00-00-2010			
4. TITLE AND SUBTITLE Detection of Dismounts using Synthetic Aperture Radar		5a. CONTRACT NUMBER			
		5b. GRANT NUMBER			
		5c. PROGRAM ELEMENT NUMBER			
6. AUTHOR(S)		5d. PROJECT NUMBER			
		5e. TASK NUMBER			
		5f. WORK UNIT NUMBER			
7. PERFORMING ORGANIZATION NAME(S) AND ADDRESS(ES) Air Force Research Laboratory, Sensors Directorate, Hanscom AFB, MA, 01731		8. PERFORMING ORGANIZATION REPORT NUMBER			
9. SPONSORING/MONITORING AGENCY NAME(S) AND ADDRESS(ES)		10. SPONSOR/MONITOR'S ACRONYM(S)			
		11. SPONSOR/MONITOR'S REPORT NUMBER(S)			
12. DISTRIBUTION/AVAILABILITY STATEMENT Approved for public release; distribution unlimited					
13. SUPPLEMENTARY NOTES See also ADM002322. Presented at the 2010 IEEE International Radar Conference (9th) Held in Arlington, Virginia on 10-14 May 2010. Sponsored in part by the Navy.					
14. ABSTRACT This paper presents an approach to detect people, or dismounts, using synthetic aperture radar (SAR). This approach is compared qualitatively with ground moving target indication (GMTI) radar and then quantitative results are presented using a P-band single phase center SAR. It is demonstrated that SAR provides an excellent methodology to detect dismounts.					
15. SUBJECT TERMS					
16. SECURITY CLASSIFICATION OF:			17. LIMITATION OF ABSTRACT	18. NUMBER OF PAGES	19a. NAME OF RESPONSIBLE PERSON
a. REPORT unclassified	b. ABSTRACT unclassified	c. THIS PAGE unclassified	Same as Report (SAR)	6	

collect is described, to include the target and radar characteristics. The algorithm and results of the experiment are then provided followed by analyses and summary.

II. GMTI AND SAR PRINCIPLES

A. GMTI Background

For radar to detect moving targets, it needs to mitigate echoes received from the natural environment (land, sea, weather, etc.). The echoes from these topographic, geologic and natural features “cluttered” early displays, and resulted in the name “clutter” to describe the competing natural interference. Clutter returns can be many orders of magnitude greater than target returns and can mask targets, especially at low Doppler frequencies. The Doppler effect is the change in frequency of the radar echo signal due to the relative velocity between the radar and a moving target.

Moving targets have a Doppler that stationary clutter does not. This represents a discriminant that can be used to pull targets out of the clutter when they appear in the same resolution cell. Note that, unlike the thermal receiver noise, the returns due to clutter are colored – which means that they have spectral preference and non-uniform content across the receiver bandwidth.

Pulsed radars that employ Doppler processing to detect moving targets fall into two general categories that use different pulse repetition frequencies (PRFs):

1. GMTI radar: low PRF with no range ambiguities (but has Doppler ambiguities).
2. Pulsed Doppler radar: high PRF to avoid Doppler ambiguities (but has range ambiguities).

Here we will focus on GMTI radar and derive the basic principals to facilitate an understanding of GMTI dismount detection.

Assume that a radar is transmitting pulses to try to detect a target a range R . The total number of wavelengths in the 2-way path from the radar to a target at range R is $2R/\lambda$, where λ is the radar wavelength. Each wavelength corresponds to a phase change of 2π radians. The total phase change in the 2-way propagation path is then,

$$\phi = 2\pi \frac{2R}{\lambda} = \frac{4\pi R}{\lambda}. \quad (1)$$

If the range R changes due to target motion, then the phase changes also. This is the Doppler effect that modifies the frequency of the signal that propagates from the radar to the target and back. As depicted in Figure 1, a moving target means that both range and phase will change due to motion. The angular frequency ω_d is the derivative of phase with respect to time (rate of change of phase),

$$\omega_d = \frac{d\phi}{dt} = \frac{4\pi}{\lambda} \frac{dR}{dt} = \frac{4\pi}{\lambda} v_r = 2\pi f_d, \quad (2)$$

where v_r is radial velocity (m/s) or rate of change of range with time and f_d is the Doppler frequency shift,

$$f_d = \frac{2v_r}{\lambda} = \frac{2f_r v_r}{c}, \quad (3)$$

with radar frequency $f_r = c/\lambda$.

Consider a radar that transmits a signal with some frequency f_i given by $A_t \sin(2\pi f_i t)$. The receive signal is then given by $A_r \sin(2\pi f_i (t - T_R))$, where the round-trip time is $T_R = 2R/c$. The target, in the notional geometry of Fig. 1, moves towards the radar, so the range is changing as $R = R_0 - v_r t$. The received signal can now be expressed by,

$$V_{rec} = A_r \sin \left[2\pi f_i \left(1 + \frac{2v_r}{c} \right) t - \frac{4\pi f_i R_0}{c} \right]. \quad (4)$$

where the frequency changes by $2f_i v_r/c = f_d$. Also, the sign of the Doppler frequency would have been negative if target had been moving away from target.

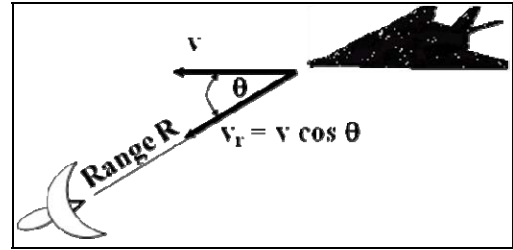


Figure 1. Notional GMTI geometry / Doppler shift

Returns from two subsequent pulse repetition periods (sweeps) can then be subtracted – stationary clutter remains the same and will cancel while moving targets change in amplitude due to Doppler frequency shift and leave a residue. This represents a simple clutter filter and other forms of filtering are used (e.g. 3 pulse canceller, STAP, etc.) Fig. 2 depicts a classic GMTI radar display.

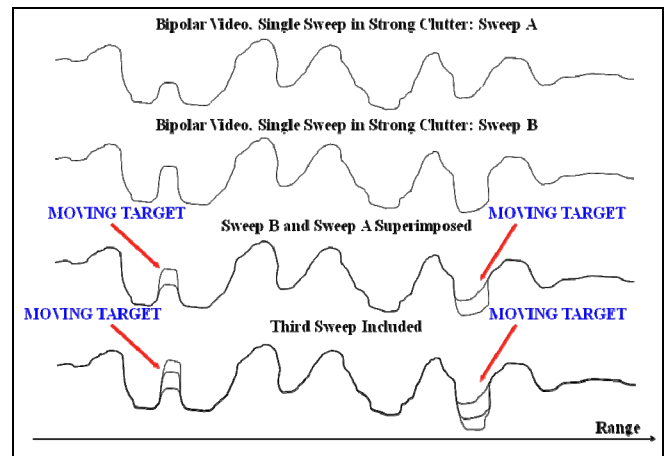


Figure 2. Classic GMTI radar display

In practice however the clutter has a Doppler bandwidth that is nonzero due to non-ideal platform motion

compensation, thus certain low velocity (low Doppler) targets (e.g. dismounts) are obscured and not detected because they fall into the clutter filter's attenuation band.

B. SAR Background

In contrast to GMTI radars, SAR [6][7] does not attempt to cancel clutter, but instead considers the clutter as the target of interest. For example, in Fig. 3 is shown a SAR image, courtesy Sandia National Laboratory, from their Mini-SAR system operating at Ku-band frequency in Albuquerque, NM. The buildings, cars, and other stationary objects focus quite clearly into a recognizable image using SAR processing. This image is particularly sharp due to the high frequency (i.e. small wavelength) used by the Mini-SAR system.



Figure 3. SAR image from a Sandia National Laboratories (SNL) Ku-band Mini-SAR. Image courtesy SNL from <http://www.sandia.gov/RADAR/sar-data.html>.

In a simplified description, SARs form images of the clutter scatterers producing a virtual map of the radar scatterers in the scene. SARs transmit many radar pulses while the radar platform traverses over a synthetic aperture such that an angular swath is covered relative to the scene center. The received samples are used to construct an image of the scene essentially using the differing Doppler shifts for each scatterer as the azimuth separation mechanism in the image formation process. Range separation is accomplished using pulse compression, as in GMTI radars.

The clutter from the SAR perspective is any moving targets. Moving targets produce smears and/or displacement in the final SAR image. Because of this, SARs have an inherent capability to detect moving targets due to the differences between moving and stationary object signatures. Also, the context provided by the image can aid target detection.

III. DISMOUNT DETECTION ALGORITHM AND SKYSAR RESULTS

We next describe the algorithm used to detect dismounts followed by the results from processing SkySAR data.

A. Detection Algorithm

The detection algorithm designed for this study can process either a standard SAR image or else a “difference”

image that has greatly reduced clutter components. The false alarm and detection performance is notably improved in the latter case, as will be discussed due to the higher signal-to-clutter ratio (S/C).

The top-level algorithm is illustrated in Fig. 4. The input SAR images are complex images, not magnitude or detected images, because the algorithm seeks to estimate the phase errors associated with moving scatterers (targets) as distinct from stationary scatterers. The difference image is formed by subtracting one complex image from another as long as they are available as co-registered to each other using precise phase alignment and by using a common ground reference point in the image formation process. The SkySAR images used were phase and registration matched in this manner such that the complex valued image pixels could be subtracted between the images without any other phase alignment steps required. More will be discussed on this topic in the sequel.

Once the single pass or difference image is formed, the next step is to segment that image into small rectangular ‘chips’, possibly overlapped. Each chip has dimension the size of the expected maximum smear size for a moving dismount, e.g. in SkySAR case it is empirically estimated to be approximately 8 range pixels by 30 azimuth pixels.

Each chip is processed sequentially in the following manner. First is a range migration removal and azimuth focus process depicted in Fig. 5. This process takes the fast Fourier transform (FFT) of the chip in the azimuth dimension (i.e. along a row), estimates the average energy location for each column (i.e., finds the energy concentration location in range), circular-shifts each column to move the average energy peak to the center range location in the chip, and lastly applies a column FFT (over range) to the modified chip. Next, the process implements an azimuth phase focusing step (discussed next), and finally implements a two-dimensional fft which converts the chip back to a standard complex image format. Now the target signature is aligned narrowly along a small number rows (ideally one) and well-focused in azimuth essentially minimizing the smear length and width.

The azimuth phase focusing step mentioned in the preceding paragraph is a variant of the shear averaging algorithm by Fienup [10][11]. Essentially, the (power-weighted) range-average of the chip's phase-gradient map (PGM) is computed. (The PGM is the instantaneous phase difference from pulse to pulse for each row.) Next, this range-averaged sequence is integrated to form the phase correction sequence, which is then conjugated and multiplied across each row of the modified chip that was outputted by the range migration step, resulting in a nonparametrically focused chip.

The degree of focusing is measured using a sharpness metric as defined similar to that of shear averaging and stored in memory as a function of chip location. The sharpness metric is compared to a user adjustable threshold. If the chip's sharpness metric exceeds the threshold then a moving target (e.g., a dismount) is declared present, otherwise it is declared not present. After all chips are processed, the detected targets are presented as synthetic dots in the center locations of the chips they are from and optionally overlaid as dots on the original SAR image for geolocation purposes.

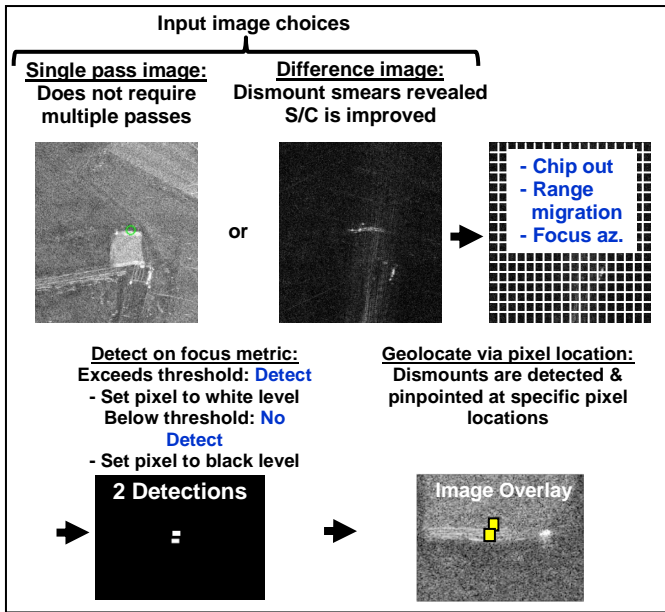


Figure 4. Dismount detection algorithm diagram.

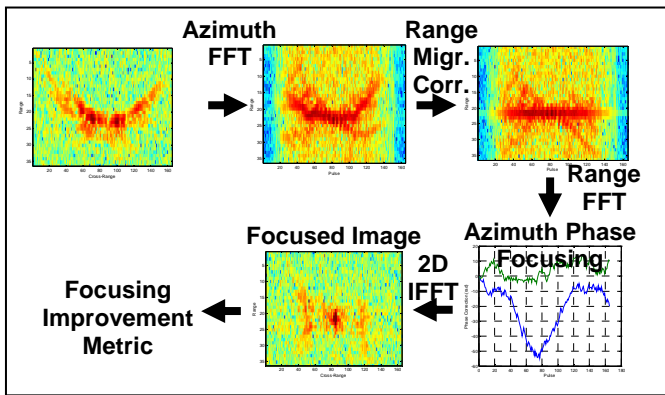


Figure 5. Range migration and Azimuth Focusing Diagram.

B. SkySAR Results

The SAR system used to collect the data processed here is a Sky Research Inc. SkySAR P-band system whose instantaneous bandwidth extends from approximately 220 MHz – 450 MHz. It is a single channel system with data taken at a nominal altitude of 10,000 feet, flown in a BAE Jetstream J31 aircraft. It is a four polarization system and has image resolution specification of approximately half-meter in range and cross range dimensions.

Data was collected October 9, 2008 in the region of a small airstrip in northern Oregon, near the Washington state border. The scene included an airstrip, vehicles, dismounts, and farmland (potentially plowed and unplowed segments). One of the dismounts had a GPS system located on his person and recording his position in one second increments for ground truth data.

The SkySAR radar was used in a controlled experiment where two dismounts were instructed to stand, walk or run in specific directions at specific times during the image collection interval.

In Fig. 6 we show a comparison of an optical image from Google Earth™, approximately matching the same image area mapped by SkySAR radar. The two images are taken several months apart and thus the plowed fields and certain objects will be different, but the primary airstrip feature is assumed the same. In addition, the SkySAR image is known to have a stationary automobile and two dismounts present in the scene as ground truth targets during the time of the collect. These are pointed out using the arrows shown, but are not present in the optical image.

One of the dismounts was instrumented with GPS to log his position during the collect interval. Both dismounts were known to be wearing normal civilian clothes, in that no extraordinarily high RCS object was attached to their bodies. The dismounts were instructed to stand still during the collection window associated with Fig. 6 and are self-evident as ‘dots’ near the automobile image (larger dot). The three dots match well the collective ground truth information regarding the experiment. The resolution of the SAR system is on the order of a human dimension, thus the stationary signatures for these targets are expected to be simple dots as shown. Clearly the SAR is able to provide a detectable image for stationary dismounts for the given clutter background.

In Fig. 7 we show another set of SkySAR images of the same area but rotated approximately 90 degrees counter clockwise from the orientation of Fig. 6. The two images are denoted as pass 1 (left) and pass 2 (right) and are taken about 15 minutes apart. The images’ range dimensions are vertical and the cross range (i.e. azimuth) dimensions are horizontal.

The pass 1 image is when the dismounts were instructed to remain stationary and the two dots match their true locations; one dot is exactly validated by the GPS as evident by the green circle placed there by a precise geolocation registration step. The other dot was validated as correct from persons familiar with the experiment. Notice the vehicle’s dot is seen in the corner of the virtual right triangle that connects all three targets, matching Fig 6.



Figure 6. Google Earth optical image (left); a corresponding SkySAR image (right), taken months apart.

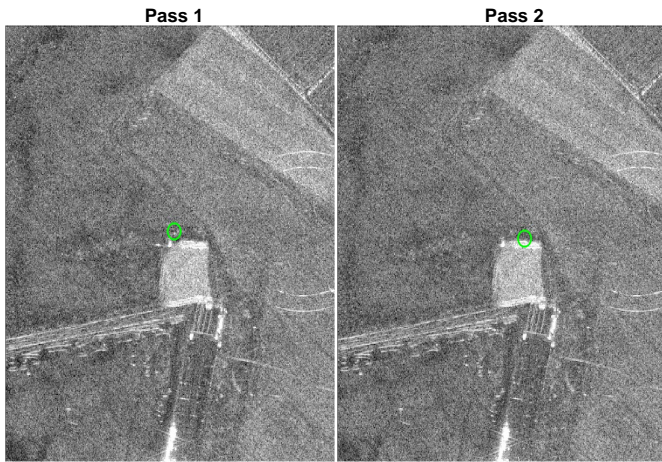


Figure 7. Two SkySAR images taken ~15 minutes apart. Left image has stationary dismounts. Right image has moving dismounts. Green circle is GPS location of one dismount half way through image collection interval.

The pass 2 image was formed when the dismounts were in motion. The green circle indicates the true position of one dismount about half way through the image data collection interval, nominally three minutes in length. The dismount motion was scheduled to be constant velocity walking and solely in the cross range direction (i.e. dismounts walked parallel to the radar platform velocity vector, however in the opposite direction).

SAR phase error theory [6] predicts a cross-range smear will be produced in this situation, namely that cross range velocity components of target motion will produce a smear effect. For completeness, any range acceleration components will also produce a smear in cross-range dimension, with differing multiplying constants, however [6]. In addition, due to the relatively close proximity of the radar platform to the scene center (~5km) the targets will experience range migration and any smear will end up generally parabolic in shape as the range between the dismount and the radar changes during the image collection interval.

Nevertheless, the dismount target smears in Fig. 7 (right) are not obvious and their location is elusive without GPS. Their smear signatures are indeed present in the complex image but obscured by the clutter in the scene, apparently hidden by some potentially plowed earth clutter which is producing a stronger backscatter RCS than the surrounding fields. By subsequent signal processing, with or without difference imaging, the target signatures may be automatically detected. As will be seen, performance is improved with differencing.

Since the two images have exquisite motion compensation and identical geo-registration, they may be subtracted coherently by differencing the complex image pixel values directly from pass 1 and pass 2 images. This results in a difference image as shown in Fig. 8 (displayed after taking the pixel magnitudes). The arrows point out the two dismount smears previously obscured by clutter in Fig. 7.

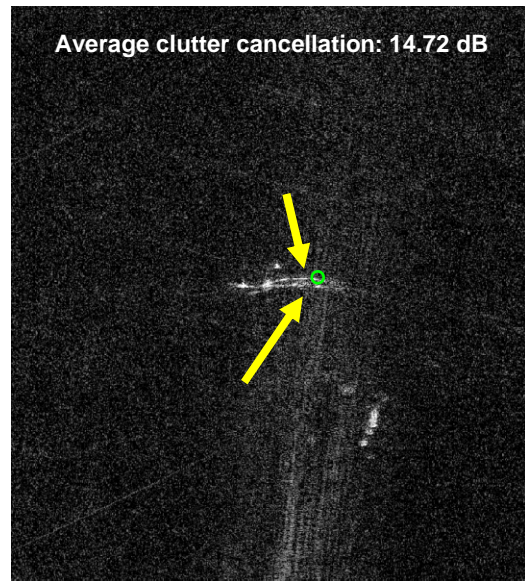


Figure 8. Difference image (shown enlarged) by coherently subtracting complex image pass 2 from complex image pass 1. Arrows point to dismount motion smears. Green circle is GPS location of dismount. Difference image results in approximately 15dB lower clutter power on average than either pass 1 or pass 2.

The top smear is validated by ground truth to be the approximate location of the instrumented dismount. The lower smear matches the approximate location and motion profile of the second dismount which is known to be matching the first dismount except by a small range difference to the radar.

In reality, human error may have imparted some range-velocity component to the overall motion profile, imparting a cross range shift of the entire smear, as predicted by SAR theory [6]. This is a possible explanation for the small difference between the location of the GPS-located green circle and the peak of the parabolic smear's shape in the cross range dimension.

Notice that the difference image has the stationary dismount and vehicle signatures (dots) present as well as the motion smears. This is predicted, i.e. the *differences* between the two images will be preserved. In addition we point out some 'bleed through' of strong clutter that perhaps scintillated or experienced a form of sidelobe leakage. Overall, however, the clutter power was measured to be approximately 15 dB lower power on average for the difference image relative to either pass 1 or pass 2 images.

Either the single pass or difference image may be inputted to the detection algorithm as illustrated in Fig. 4. We next show an example of the detection performance using both forms of input images.

In Fig. 9 we show detection performance using as input the difference image shown in Fig. 8. With no false alarms, the algorithm correctly detects and locates one of the two dismounts and likely collapsed the second dismount detection

into the first because of their proximity to one another. This represents an empirical measure of the resolution of the detection algorithm. When the dismounts are separated by the order of the SAR image resolution (a pixel), as they are in Fig. 8, the algorithm may not be able to separate them. However this represents an extreme case in that many situations will have dismounts separated by more distance.

Notice the clutter bleed through did not effect the detection performance since the azimuth focusing and range migration steps differentiated the dismount motion vs. other forms of stationary scatterer phase functions. The algorithm's detection threshold was set empirically to match the data set provided. More research is needed to automatically set this threshold.

In Fig. 10 we show results for the single pass input case. We see that the algorithm correctly detects both dismounts, but, for the choice of threshold chosen, there were eight false alarms. It is possible these are due to clutter bleed-through, or even due to moving scatterers that were not known to be present in the scene. The choice of using a difference image has a dramatic impact on the false alarm performance but in either case there is reasonable performance for detection of dismounts. It is felt further refinements to the algorithm will improve the performance for both cases of inputs.

We highlight that the dismount motion signatures fall within the clutter's Doppler bandwidth by virtue of the fact that clutter competes with the motion smears (as seen visually in the results presented here). GMTI radars would not be able to detect these targets because the clutter filter used (either a GMTI or STAP filter) will not pass the dismount signal to the detector processor because these filters attenuate all clutter Doppler components.

In contrast, the SAR-based dismount detection technique presented here illustrates that the form of SAR data is indeed suitable for subsequent filtering of dismount signals even though the signatures appear clutter limited in the case of a single pass input image. For the case of using a difference image, the clutter is mostly attenuated to begin with and better performance is evident.

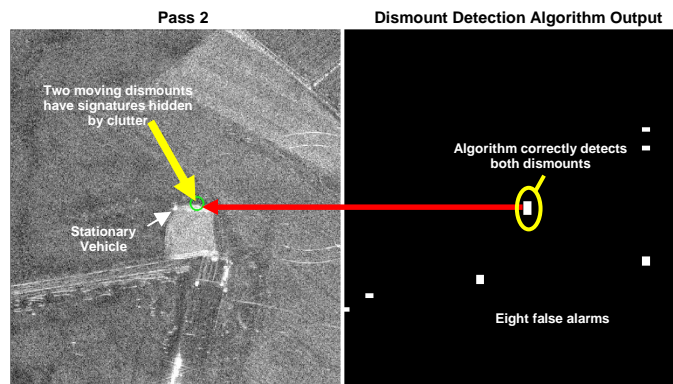


Figure 10. Single pass (pass 2) input image (left); corresponding dismount detection image (right). Both dismounts detected; eight false alarms.

IV. CONCLUSIONS

We present a signal processing technique to detect dismounts using synthetic aperture radar. GMTI and SAR systems are discussed in a qualitative manner indicating the suitability of SAR over GMTI for this purpose. Quantitative results are presented using a P-band single phase center SAR by processing experimental data and validated with dismount ground truth information. It is demonstrated that dismount signatures are present in SAR data and reliably detectable with suitable signal processing algorithms.

REFERENCES

- [1] Schleher, C. (1999). MTI and Pulsed Doppler Radar, Boston: Artech House.
- [2] Skolnik, M. (2003). Introduction to Radar Systems, 3rd ed., New York: McGraw Hill.
- [3] Brennan, L. E., Reed, I. S., "Theory of Adaptive Radar", IEEE Trans. Aerospace and Electronic Systems, Vol. AES-9, No. 2, March 1973, pp. 237-252.
- [4] Ward, J., "Space-Time Adaptive Processing for Airborne Radar", MIT Lincoln Laboratory Technical Report 1015, Lexington, Mass., Dec. 13, 1994.
- [5] Haykin, .S., Adaptive Filter Theory, 3rd Ed., Prentice Hall, New Jersey, 1996.
- [6] Carrara, W.G., Majewski, R.M., Goodman, R.S., *Spotlight Synthetic Aperture Radar: Signal Processing Algorithms*, Artech House, 1995.
- [7] Soumekh, M (1999). Synthetic Aperture Radar Signal Processing - with Matlab Algorithms, New York: John Wiley and Sons.
- [8] Hersey, R.K., Melvin, W.L., and Culpepper, E. (2008). Dismount Modeling and Detection from Small Aperture Moving Radar Platforms. IEEE Radar Conference, May 2008, pages 1-6.
- [9] Van Dorp, P., and Groen, F.C.A.. (2003). Human walking estimation with radar. IEE Proceedings Radar, Sonar, Navig. Vol 150, No. 5, Oct.
- [10] J.R. Fienup, "Phase Error Correction by Shear Averaging", Signal Recovery and Synthesis III, Optical Society of America, June 1989, pp. 134-137
- [11] J.R. Fienup, A.M. Kowalczyk, "Detecting Moving Targets in SAR Imagery by Using a Phase-Error Correction Algorithm", SPIE Vol. 2487, pp. 337-343.

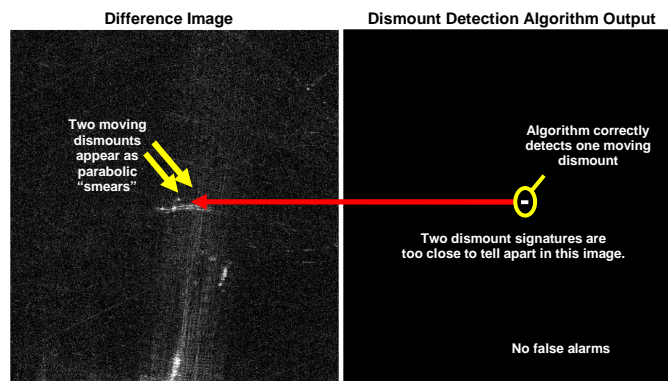


Figure 9. Difference input image (left); corresponding dismount detection image (right). Two dismounts detected as one due to proximity to each other; no false alarms.